The Astrophysical Journal Letters, 737:L37 (6pp), 2011 August 20 doi:10.1088/2041-8205/737/2/L37

THROUGH THICK AND THIN—H I ABSORPTION IN COSMOLOGICAL SIMULATIONS

Gabriel Altay[1], Tom Theuns[1,2], Joop Schaye[3], Neil H. M. Crighton[4,5], and Claudio Dalla Vecchia[3,6]
[1] Institute for Computational Cosmology, Department of Physics, Durham University, South Road, Durham, DH1 3LE, UK; gabriel.altay@gmail.com
[2] Department of Physics, University of Antwerp, Campus Groenenborger, Groenenborgerlaan 171, B-2020 Antwerp, Belgium
[3] Leiden Observatory, Leiden University, P.O. Box 9513, 2300 RA Leiden, The Netherlands
[4] Department of Physics, University of Durham, South Road, Durham DH1 3LE, UK
[5] Max Planck Institute for Astronomy, Königstuhl 17, D-69117 Heidelberg, Germany
[6] Max-Planck-Institut für Extraterrestrische Physik, Giessenbachstraße, D-85478 Garching, Germany
Received 2010 December 17; accepted 2011 July 18; published 2011 August 2

ABSTRACT

We investigate the column density distribution function of neutral hydrogen at redshift $z = 3$ using a cosmological simulation of galaxy formation from the OverWhelmingly Large Simulations project. The base simulation includes gravity, hydrodynamics, star formation, supernovae feedback, stellar winds, chemodynamics, and element-by-element cooling in the presence of a uniform UV background. Self-shielding and formation of molecular hydrogen are treated in post-processing, without introducing any free parameters, using an accurate reverse ray-tracing algorithm and an empirical relation between gas pressure and molecular mass fraction. The simulation reproduces the observed $z = 3$ abundance of Lyα forest, Lyman limit, and damped Lyα H I absorption systems probed by quasar sight lines over 10 orders of magnitude in column density. Self-shielding flattens the column density distribution for $N_{\rm H\,I} > 10^{18}$ cm^{-2}, while the transition to fully neutral gas and conversion of H I to H$_2$ steepen it around column densities of $N_{\rm H\,I} = 10^{20.3}$ cm^{-2} and $N_{\rm H\,I} = 10^{21.5}$ cm^{-2}, respectively.

Key words: galaxies: formation – intergalactic medium – large-scale structure of universe – methods: numerical – quasars: absorption lines

Online-only material: color figures

1. INTRODUCTION

Ground-based spectroscopic observations targeting quasars are excellent probes of $z \geqslant 1.7$ neutral hydrogen (e.g., Rauch 1998; Wolfe et al. 2005). The Sloan Digital Sky Survey (SDSS) has produced approximately 1.5×10^4 moderate resolution quasar spectra (Abazajian et al. 2009). These spectra provide ample data on H I absorption lines with column densities $N_{\rm H\,I} > 10^{20.3}$ cm^{-2}, the so-called damped Lyα systems (DLAs; Prochaska & Wolfe 2009; Noterdaeme et al. 2009). Lines with $N_{\rm H\,I} < 10^{17.2}$ cm^{-2}, the so-called Lyα forest, are best discovered in high-resolution spectra of bright quasars (e.g., Kim et al. 2002). Lines with intermediate column densities, Lyman limit systems (LLSs), lie on the flat part of the curve of growth, which complicates the determination of their column densities. Traditional methods of measuring $N_{\rm H\,I}$ in DLAs can be applied to high-resolution spectra for lines with $N_{\rm H\,I} > 10^{19}$ cm^{-2} when damping wings begin to appear (e.g., Péroux et al. 2005; O'Meara et al. 2007). Progress on the most difficult lines with $10^{14.5}$ cm^{-2} $< N_{\rm H\,I} < 10^{19}$ cm^{-2} has recently been made by Prochaska et al. (2010) by combining independent measurements of the Lyman limit mean free path and integral constraints over the column density distribution.

Combining the observations above, one can determine the H I column density distribution function $f(N_{\rm H\,I}, z)$, i.e., the number of lines per unit column density $dN_{\rm H\,I}$, per unit absorption distance dX, at redshifts $z \approx 3$ from $N_{\rm H\,I} = 10^{12}$ cm^{-2} to $N_{\rm H\,I} = 10^{22}$ cm^{-2}. Early determinations of $f(N_{\rm H\,I}, z)$ at these redshifts were reasonably well described by a single power law, $f(N_{\rm H\,I}, z) \propto N_{\rm HI}^{-\eta}$, with $\eta = 1.5$ (Tytler 1987). As the quality of observations improved, this was no longer the case. Petitjean et al. (1993) showed that a single power law and a double power law with a break at $N_{\rm H\,I} = 10^{16}$ cm^{-2} both failed Kolmogorov–Smirnov tests at the 99% confidence level. The most recent observations are fit well by a series of six power laws which intersect at $N_{\rm H\,I} = \{10^{14.5}, 10^{17.3}, 10^{19.0}, 10^{20.3}, 10^{21.75}\}$ cm^{-2} (Prochaska et al. 2010).

Attempts to explain the shape and normalization of $f(N_{\rm H\,I}, z)$ in a cosmological context have typically focused on subsets of the full column density range. Analytic (e.g., Schaye 2001a), semi-analytic (e.g., Bi & Davidsen 1997), and numerical (e.g., Theuns et al. 1998a, 1998b) models were instrumental in identifying the Lyα forest lines with the diffuse, photoionized, intergalactic medium. Numerical work has also played a large role in determining properties of higher column density systems (e.g., Katz et al. 1996; Gardner et al. 1997; Haehnelt et al. 1998; Cen et al. 2003; Nagamine et al. 2004; Razoumov et al. 2006; Kohler & Gnedin 2007; Pontzen et al. 2008; Tescari et al. 2009; Hong et al. 2010; Cen 2010; Nagamine et al. 2010; McQuinn et al. 2011).

Although self-shielding is crucial for modeling optically thick absorbers, only Razoumov et al. (2006), Kohler & Gnedin (2007), Pontzen et al. (2008), and McQuinn et al. (2011) have used three-dimensional radiative transfer to calculate the attenuation of the UV background. Additionally, conversion of H I to H$_2$ is thought to determine the high end cutoff in $f(N_{\rm H\,I}, z)$ (Schaye 2001b; Krumholz et al. 2009), yet only Cen (2010) included this process when modeling H I absorption. We present a cosmological simulation of structure formation, to which we have applied a radiative transfer self-shielding calculation and a prescription for the conversion of H I to H$_2$ without introducing any free parameters. We show that this simulation reproduces observational determinations of $f(N_{\rm H\,I}, z)$ around $z = 3$ over the entire range in column density. In addition, we determine the typical neutral fractions and total hydrogen number densities for H I absorbers as a function of column density $N_{\rm H\,I}$.

2. METHODOLOGY

We focus on model *REF_WMAP7_L025N512* from the OverWhelmingly Large Simulations (OWLS) project (Schaye et al. 2010), which is identical to *REF_L025N512* except that it was run using *WMAP7* cosmological parameters. This simulation was performed with a modified version of the smoothed particle hydrodynamics (SPH) code GADGET (Springel 2005), and includes "sub-grid" models for star formation (Schaye & Dalla Vecchia 2008), chemodynamics (Wiersma et al. 2009a), galactic winds (Dalla Vecchia & Schaye 2008), and element-by-element cooling in the presence of a uniform UV background (Wiersma et al. 2009b). Gas in the interstellar medium (ISM) at densities above $n_{\rm H}^* = 0.1\,{\rm cm}^{-3}$ is assumed to be multi-phase and star-forming. This is modeled by imposing a polytropic equation of state (EoS) of the form $P = P_*(n_{\rm H}/n_{\rm H}^*)^{4/3}$. Because surface density and pressure are directly related in self-gravitating systems, the Kennicutt–Schmidt star formation law can be rewritten as a pressure law (Schaye & Dalla Vecchia 2008). The observed Kennicutt–Schmidt law can then be used to determine a star formation rate in each gas particle.

The simulation contains 2×512^3 particles in a periodic cube of size 25 comoving h^{-1} Mpc. The cosmological parameters used are $\{\Omega_{\rm m} = 0.272,\ \Omega_{\rm b} = 0.0455,\ \Omega_\Lambda = 0.728,\ \sigma_8 = 0.81,\ n_{\rm s} = 0.967,\ h = 0.704\}$ (Komatsu et al. 2011). The mass resolution is $m_{\rm b} = 1.47 \times 10^6\,h^{-1}\,M_\odot$ and $m_{\rm dm} = 7.32 \times 10^6\,h^{-1}\,M_\odot$ for baryonic and dark matter particles, respectively. The equivalent Plummer gravitational softening length is $\epsilon(z) = 1.95/(1+z)$ proper h^{-1} kpc at high z but is not allowed to exceed 0.5 proper h^{-1} kpc, a value reached at $z = 2.91$.

REF_WMAP7_L025N512 included the (Haardt & Madau 2001, hereafter HM01) optically thin UV background from quasars and galaxies, but we apply a self-shielding correction in post-processing as follows. For each particle, we trace rays out to a distance $l_{\rm ray}$ along $N_{\rm ray}$ directions defined using the HEALPix algorithm (Górski et al. 2005). We then compute frequency-dependent optical depths along each ray and integrate over the HM01 spectrum to calculate a self-shielded photoionization rate, $\Gamma^{\rm shld}$, as opposed to the optically thin rate, $\Gamma_{12}^{\rm thin} = \Gamma^{\rm thin}/10^{-12}\ {\rm s}^{-1} = 1.16$. This characterizes each particle with an effective optical depth $\tau_{\rm eff} = -\ln(\Gamma^{\rm shld}/\Gamma^{\rm thin})$. We then use $\Gamma^{\rm shld}$ to calculate a new neutral fraction, $x_{\rm H\,I} = n_{\rm H\,I}/n_{\rm H}$, for each particle using an analytic equilibrium solution. We continue to loop over the particles until the neutral fractions converge. We obtain converged results for $f(N_{\rm H\,I}, z)$ using $l_{\rm ray} = 100$ proper kpc and $N_{\rm ray} = 12$. Our self-shielding algorithm will be discussed in detail elsewhere (G. Altay et al. 2011, in preparation).

In the OWLS snapshots, the temperature stored for gas particles on the polytropic star-forming EoS is simply a measure of the imposed effective pressure. When calculating collisional ionization and recombination rates, we set the temperature of these particles to $T_{\rm ISM} = 10^4$ K. This temperature is typical of the warm-neutral medium phase of the ISM but our results do not change if we use lower values. We use case A (B) recombination rates for particles with $\tau_{\rm eff} < (>) 1$. In addition, the optically thin approximation used in the hydrodynamic simulation leads to artificial photo-heating by the UV background in self-shielded particles. To compensate for this, we enforce a temperature ceiling of $T_{\rm shld} = 10^4$ K in those particles that become self-shielded (i.e., attain $\tau_{\rm eff} > 1$). In Figure 2 we show the effect of this temperature correction.

For conversion of atomic hydrogen to molecules, we adopt a prescription based on observations by Blitz & Rosolowsky (2006) of 14 local spiral galaxies to form an H_2-fraction–pressure relation. Their sample includes various morphological types and spans a factor of five in mean metallicity. They obtain a power-law scaling of the molecular fraction, $R_{\rm mol} \equiv \Sigma_{\rm H_2}/\Sigma_{\rm H\,I}$, with the galactic mid-plane pressure, $R_{\rm mol} = (P_{\rm ext}/P_0)^\alpha$, with $\alpha = 0.92$ and $P_0/k_{\rm b} = 3.5 \times 10^4\ {\rm cm}^{-3}$ K. Applying this relation to the simulated ISM yields $f_{\rm H_2} = [1 + A(n_{\rm H}/n_{\rm H}^*)^{-\beta}]^{-1}$ with $A = (P_*/P_0)^{-\alpha}$, and $\beta = \alpha\gamma_{\rm eff}$.

The H I column density distribution function,

$$f(N_{\rm H\,I}, z) \equiv \frac{d^2 n}{dN_{\rm H\,I}\,dX} \equiv \frac{d^2 n}{dN_{\rm H\,I}\,dz}\frac{dz}{dX}, \qquad (1)$$

is defined as the number of absorption lines n, per unit column density $dN_{\rm H\,I}$, per unit absorption distance dX. The latter is related to redshift path dz as $dX/dz = H_0(1+z)^2/H(z)$, where $H(z)$ is the Hubble parameter (Bahcall & Peebles 1969). In the comparisons below, we scale $f(N_{\rm H\,I}, z)$ reported by various observers to the cosmology assumed in our simulation.

The simulated $f(N_{\rm H\,I}, z)$ below $N_{\rm H\,I} = 10^{17}\ {\rm cm}^{-2}$ is computed by generating 1000 mock spectra through each snapshot. We then apply instrumental broadening with FWHM 6.6 km s^{-1}, add Gaussian noise such that we have a signal-to-noise ratio of 50 in the continuum, and fit the mock spectra using VPFIT (Carswell et al. 1987); see Theuns et al. (1998b) for more details. To obtain $f(N_{\rm H\,I}, z)$ for the rarer systems with $N_{\rm H\,I} \geqslant 10^{17}\ {\rm cm}^{-2}$, we project all 512^3 gas particles along the z-axis onto a grid with 16,384^2 pixels using Gaussian approximations to their SPH smoothing kernels. This leads to hypothetical lines of sight with a transverse spacing of 381 proper h^{-1} pc or about 3/4 the gravitational softening length at $z = 3$. We have verified that our results are converged with respect to the projected grid resolution. For systems with $N_{\rm H\,I} > 10^{17.5}\ {\rm cm}^{-2}$ and redshifts $z < 4.4$, the rate of incidence per unit absorption distance, $l(X)$, is observed to be less than 1 (Prochaska et al. 2010). The absorption distance for a single sight line through our box at $z = 3$ is $\Delta X_1 = 0.133$ and so we expect, on average, much less than one system per sight line. Therefore, the contribution to the total column density in projected pixels with $N_{\rm H\,I} > 10^{17.5}\ {\rm cm}^{-2}$, for the vast majority of cases, is dominated by the single absorption system in the line of sight. Curves in Figure 1 are labeled either "VPFIT" or "Projected," depending on the method used, all others were calculated using projections.

Table 1 lists the $N_{\rm H\,I}$ bins, absorption lines per bin, and total absorption distance used for the low and high $N_{\rm H\,I}$ analyses of our fiducial model. The $(25\ h^{-1}\,{\rm Mpc})^3$ volume searched for absorbers contains ≈39,000 friends-of-friends dark matter halos with masses above $7.32 \times 10^8\ h^{-1}\ M_\odot$ and yields $\approx 2 \times 10^6$ lines of sight containing DLAs. The size of this data set obviates the need to re-weight a limited sample of absorbers using an analytic mass function as in Gardner et al. (1997) or Pontzen et al. (2008).

3. RESULTS

3.1. Full Range

In Figure 1, our fiducial model $f(N_{\rm H\,I}, z)$ is plotted at $z = 3$ from $N_{\rm H\,I} = 10^{12}$–$10^{22}\ {\rm cm}^{-2}$. The analysis using VPFIT in the Lyα forest range, where self-shielding and H_2 are not important, joins smoothly onto the projection analysis at $N_{\rm H\,I} > 10^{17}\ {\rm cm}^{-2}$. The model is compared to high-resolution observations of the Lyα forest (Kim et al. 2002) and LLSs (Péroux et al.

Table 1
Simulation Line List

VPFIT $1000 \times \Delta X_1 = 133.1$		Projection $16,384^2 \times \Delta X_1 = 3.574 \times 10^7$			
$\Delta \log N_{\rm H\,I}$	No. of Lines	$\Delta \log N_{\rm H\,I}$	No. of Lines	$\Delta \log N_{\rm H\,I}$	No. of Lines
12.50–12.75	3598	17.00–17.10	858,492	20.00–20.10	314,774
12.75–13.00	4062	17.10–17.20	747,955	20.10–20.20	309,333
13.00–13.25	4135	17.20–17.30	658,685	20.20–20.30	302,340
13.25–13.50	3651	17.30–17.40	582,018	20.30–20.40	291,816
13.50–13.75	2918	17.40–17.50	518,006	20.40–20.50	275,818
13.75–14.00	2144	17.50–17.60	468,662	20.50–20.60	254,368
14.00–14.25	1362	17.60–17.70	431,614	20.60–20.70	228,520
14.25–14.50	842	17.70–17.80	406,575	20.70–20.80	198,641
14.50–14.75	466	17.80–17.90	387,631	20.80–20.90	167,671
14.75–15.00	254	17.90–18.00	374,532	20.90–20.00	135,412
15.00–15.25	145	18.00–18.10	359,789	21.00–21.10	103,583
15.25–15.50	73	18.10–18.20	350,348	21.10–21.20	76,751
15.50–15.75	49	18.20–18.30	342,146	21.20–21.30	54,326
15.75–16.00	40	18.30–18.40	334,534	21.30–21.40	37,745
16.00–16.25	25	18.40–18.50	329,178	21.40–21.50	25,140
16.25–16.50	19	18.50–18.60	324,411	21.50–21.60	16,784
16.50–16.75	11	18.60–18.70	320,648	21.60–21.70	10,938
		18.70–18.80	318,207	21.70–21.80	6,740
		18.80–18.90	316,232	21.80–21.90	3,667
		18.90–19.00	314,852	21.90–22.00	1,614
		19.00–19.10	314,504	22.00–22.10	637
		19.10–19.20	314,583	22.10–22.20	206
		19.20–19.30	313,942	22.20–22.30	33
		19.30–19.40	315,802	22.30–22.40	14
		19.40–19.50	316,330	22.40–22.50	7
		19.50–19.60	316,884		
		19.60–19.70	317,336		
		19.70–19.80	317,979		
		19.80–19.90	316,526		
		19.90–20.00	317,212		

2005; O'Meara et al. 2007), DLA statistics from the SDSS (Noterdaeme et al. 2009), and a series of best-fit power laws (Prochaska et al. 2010).

Both our model $f(N_{\rm H\,I}, z)$ and the observations display a characteristic flattening above the transition to LLSs at $N_{\rm H\,I} = 10^{17.2}\,{\rm cm}^{-2}$ and a steepening beginning around the DLA transition, $N_{\rm H\,I} > 10^{20.3}\,{\rm cm}^{-2}$. To quantify this model's goodness of fit to the data, we calculate χ^2 per degree of freedom between the model and the three largest data sets using the error bars reported by the observers. The corresponding Poisson error bars for our model are smaller than the thickness of the curves shown in Figure 1. The results are 1.26 for the Lyα forest data from Kim et al. (2002) and 1.26 and 2.24 for DLA data from Prochaska & Wolfe (2009) and Noterdaeme et al. (2009), respectively. Lower normalizations of the UV Background as found in Haardt & Madau (2011) and shown in Figure 2 would improve these fits.

3.2. LLSs and DLAs

In the left panel of Figure 2 we show models in which the amplitude of the UV background was varied by factors of three, a model with no self-shielding, and our fiducial model. Although systems with $N_{\rm H\,I} > 10^{17.2}\,{\rm cm}^{-2}$ are optically thick to photons at the Lyman limit, models with and without self-shielding (at the fiducial UV background normalization) do not diverge until $N_{\rm H\,I} = 10^{18}\,{\rm cm}^{-2}$. This is because higher energy photons with smaller cross-sections for absorption penetrate the clouds. Between $N_{\rm H\,I} = 10^{17}\,{\rm cm}^{-2}$ and $N_{\rm H\,I} = 10^{18}\,{\rm cm}^{-2}$, the model *with* self-shielding predicts *fewer* lines, because systems are moved to higher column densities in the self-shielded model.

Above $N_{\rm H\,I} = 10^{18}\,{\rm cm}^{-2}$, the model that neglects self-shielding stays on the Lyα forest power law until it steepens around $N_{\rm H\,I} = 10^{21.5}\,{\rm cm}^{-2}$ due to the formation of molecules. The other models flatten due to self-shielding and then steepen due to both the formation of molecules and the saturation of the neutral fraction. The flattening of $f(N_{\rm H\,I}, z)$ is a hallmark of self-shielding and was also found in the original numerical work of Katz et al. (1996) and in the analytic work of Zheng & Miralda-Escudé (2002). Changes in the UV background normalization by factors of three result in constant shifts of $f(N_{\rm H\,I}, z)$ until the gas is completely shielded around $N_{\rm H\,I} = 10^{21.5}\,{\rm cm}^{-2}$. This normalization adjustment is larger than any of the uncertainties claimed in recent work (e.g., Faucher-Giguère et al. 2008).

3.3. DLAs

In the right panel of Figure 2, we isolate the effects of H_2 and the photo-heating of self-shielded gas. The models with H_2 approach a vertical asymptote just above $N_{\rm H\,I} = 10^{22.0}\,{\rm cm}^{-2}$ while the model without H_2 predicts the existence of systems out to $N_{\rm H\,I} = 10^{24.5}\,{\rm cm}^{-2}$ although at such low abundance that less than one would have been discovered in the SDSS.

The introduction of H_2 produces a steepening of $f(N_{\rm H\,I}, z)$ around $N_{\rm H\,I} = 10^{21.5}\,{\rm cm}^{-2}$. Such a transition, suggested theoretically in Schaye (2001b), has been observed at $z = 0$ using CO maps as a tracer for H_2 (e.g., Zwaan & Prochaska 2006). This feature coincides with the break in the double power law

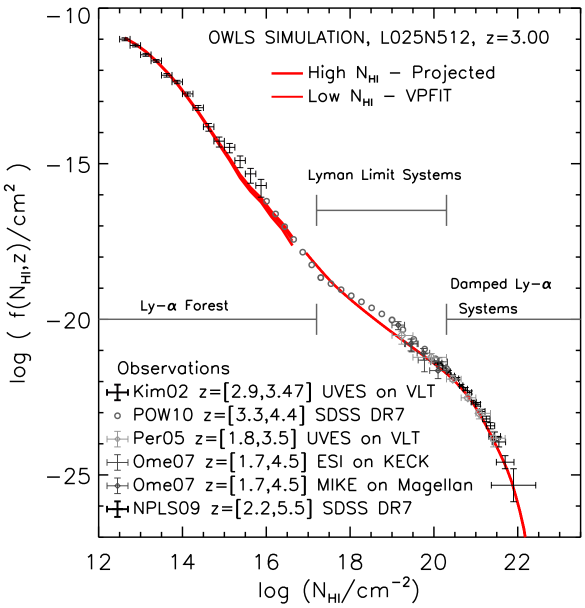

Figure 1. H I column density distribution function, $f(N_{\rm H\,I}, z)$, at $z \sim 3$; simulation results are shown as curves and observational data as symbols. The low $N_{\rm H\,I}$ curve is obtained using mock spectra fitted with VPFIT. Self-shielding and H_2 are unimportant in this range. The high $N_{\rm H\,I}$ curve is obtained by projecting the simulation box onto a plane and includes self-shielding and H_2. The gap around $N_{\rm H\,I} \sim 10^{17}$ cm^{-2} separates low and high $N_{\rm H\,I}$. Poisson errors on the simulation curves are always smaller than their thickness. We also show high-resolution observations of the Lyα forest (Kim et al. 2002, "Kim02"), LLSs (Péroux et al. 2005, "Per05"; O'Meara et al. 2007, "Ome07"), analysis of SDSS DLA data (Noterdaeme et al. 2009, "NPLS09"), and power-law constraints (Prochaska et al. 2010, "POW10"; open circles are spaced arbitrarily along power-law segments and do not represent $N_{\rm H\,I}$ bins or errors).

(A color version of this figure is available in the online journal.)

commonly used to fit $f(N_{\rm H\,I}, z)$ in the DLA column density range (Prochaska & Wolfe 2009; Noterdaeme et al. 2009), suggesting a relationship between the two. At DLA column densities, ionizing radiation from local sources may play a role (Schaye 2006). We have not included these sources in our self-shielding model, but Nagamine et al. (2010) have recently shown that $f(N_{\rm H\,I}, z)$ changes by less than 0.1 dex when local sources are included.

Because the UV background suppresses cooling, the temperature recorded in the OWLS snapshots for particles that are identified as self-shielded in post-processing is an overestimate. To compensate for this, we enforce a temperature ceiling of $T_{\rm shld} = 10^4$ K in self-shielded particles in our fiducial model. The curve labeled "w/o $T_{\rm shld}$" shows a model in which we have not performed this temperature adjustment. Because the temperature dependence of the collisional equilibrium neutral fraction is very small below 10^4 K, the two temperature models should bracket the neutral fractions one would expect from a more accurate treatment of the temperature. The difference between these two models is about a factor of 10 smaller than the difference between the optically thin and self-shielded models but can be on the order of the observational 1σ error bars around the DLA threshold where the data are most abundant. We plan to explore hydrodynamic simulations that include self-shielding in future work.

3.4. *Physical Properties of High $N_{\rm H\,I}$ Absorbers*

Neutral hydrogen mass weighted values for the neutral fraction, $x_{\rm H\,I} \equiv n_{\rm H\,I}/n_{\rm H}$, and total hydrogen number density, $n_{\rm H} = n_{\rm H\,I} + n_{\rm H\,II} + 2n_{\rm H_2}$ are plotted as a function of $N_{\rm H\,I}$ in Figure 3. The effects of self-shielding produce a steep deviation from the optically thin power law in $x_{\rm H\,I}$ above $N_{\rm H\,I} = 10^{17}$ cm^{-2}. As the UV Background normalization is reduced, and as higher temperatures are used, the deviation becomes smaller. The median $x_{\rm H\,I}$ at $N_{\rm H\,I} = 10^{18}$ cm^{-2} in our fiducial model is 0.3, however there is a large spread in the data in this column density range. It begins to drop around

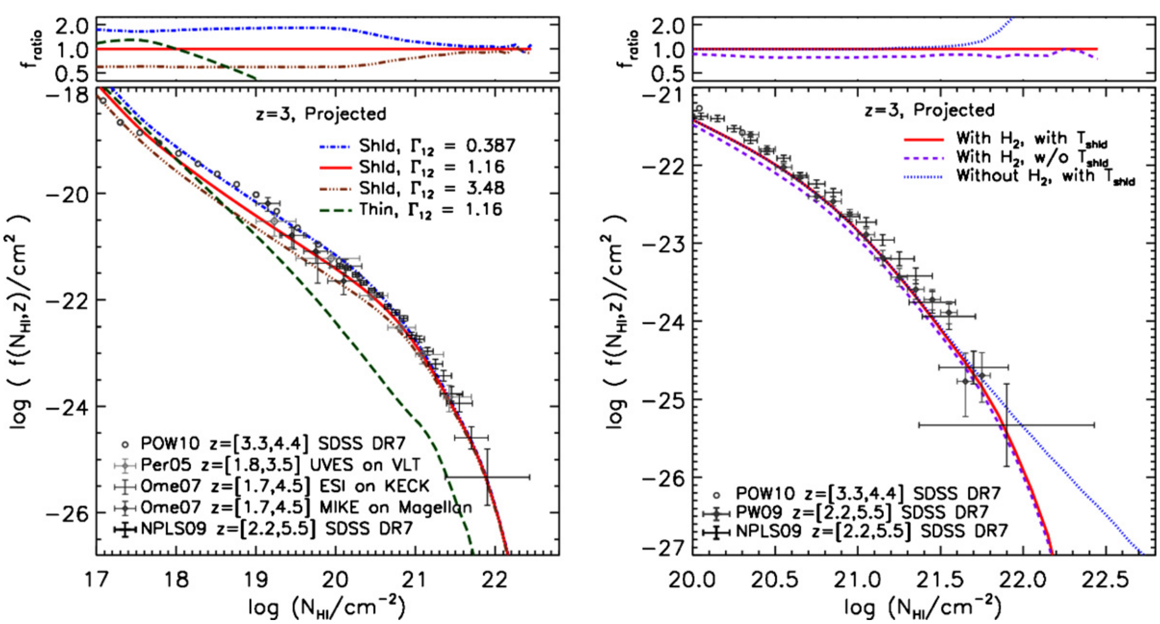

Figure 2. $f(N_{\rm H\,I}, z)$—LLS and DLA range. In the left panel, we vary the amplitude of the UV background and show the impact of neglecting self-shielding. In the right panel, we isolate the effects of H_2 and show a model in which we have not lowered the temperature in self-shielded particles (w/o $T_{\rm shld}$). On top of each panel, we show the ratio of each model to our fiducial model (solid red curve), which includes self-shielding and H_2. The observational data are a subset of those in Figure 1 plus SDSS analysis from Prochaska & Wolfe (2009, "PW09") in the right panel. Self-shielding becomes important for $N_{\rm H\,I} \geqslant 10^{18}$ cm^{-2} leading to a flattening of $f(N_{\rm H\,I}, z)$. Cooling the self-shielded gas yields a constant offset while H_2 becomes important above column densities of $N_{\rm H\,I} > 10^{21.5}$.

(A color version of this figure is available in the online journal.)

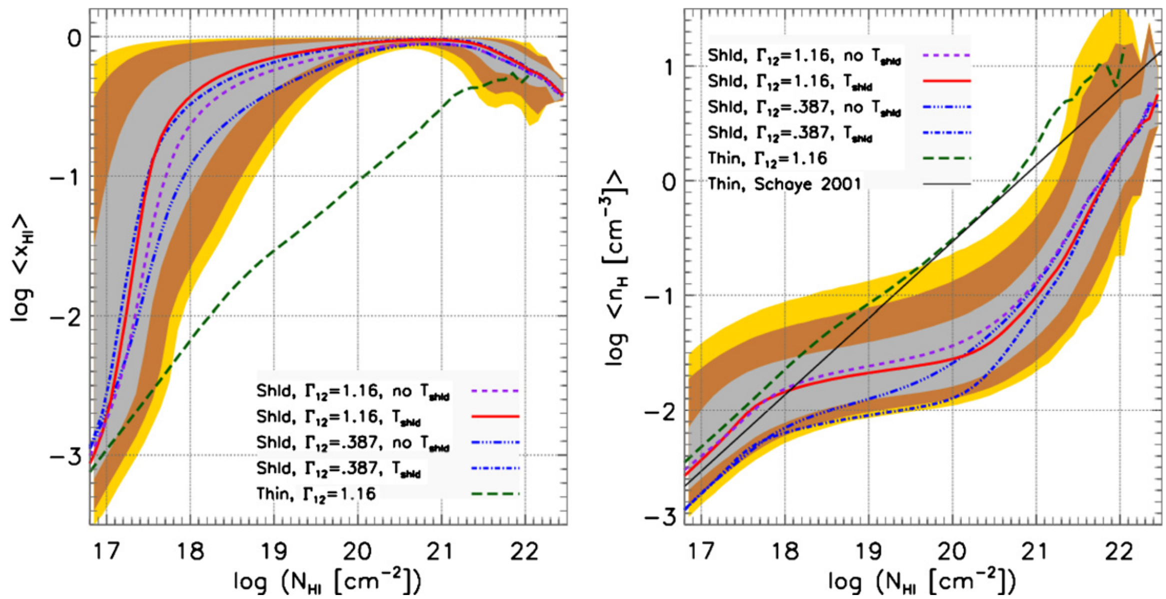

Figure 3. Left panel: $n_{\rm H\,I}$ weighted neutral fraction, $x_{\rm H\,I}(N_{\rm H\,I})$. The red solid line indicates median values in $N_{\rm H\,I}$ bins for the fiducial model which includes self-shielding and H_2. The contours represent 68%, 95%, and 99% of the data about this median in each bin. Also shown are median values for the models shown in Figure 2 and a model with lower UV background normalization and no temperature adjustment for self-shielded gas. Right panel: same as left panel, but for the $n_{\rm H\,I}$ weighted total hydrogen number density $n_{\rm H} = n_{\rm H\,I} + n_{\rm H\,II} + 2n_{\rm H_2}$. We also show the predictions of the analytic, optically thin model of Schaye (2001a). H_2 begins to reduce $x_{\rm H\,I}$ around the DLA threshold, $N_{\rm H\,I} = 10^{20.3}\,{\rm cm}^{-2}$ and self-shielding flattens the median $n_{\rm H}$ compared to the optically thin case between $10^{18}\,{\rm cm}^{-2} < N_{\rm H\,I} < 10^{20.5}\,{\rm cm}^{-2}$.

(A color version of this figure is available in the online journal.)

$N_{\rm H\,I} = 10^{21}\,{\rm cm}^{-2}$ due to the formation of H_2. Systems above $N_{\rm H\,I} = 10^{22}\,{\rm cm}^{-2}$ have lost much of their atomic hydrogen to molecules, however the H_2 likely has a small covering fraction.

The median $n_{\rm H}$ flattens around the beginning of the LLS range, $N_{\rm H\,I} = 10^{17.2}\,{\rm cm}^{-2}$, to approximately $2 \times 10^{-2}\,{\rm cm}^{-3}$ where it remains roughly constant until the start of the DLA range, $N_{\rm H\,I} = 10^{20.3}\,{\rm cm}^{-2}$. Above this column density, the gas is fully neutral (see left panel) causing $n_{\rm H}$ to rise steeply with $N_{\rm H\,I}$ and $f(N_{\rm H\,I}, z)$ to steepen (see Figure 2). Above $N_{\rm H\,I} = 10^{21}\,{\rm cm}^{-2}$, the medians for models which include H_2 are steeper than linear due to the formation of molecules. The normalization of the UV Background and the treatment of temperature can change the LLS characteristic density by half a decade. For the optically thin case we find excellent agreement with the corresponding prediction in Schaye (2001a).

4. CONCLUSIONS

We have used a hydrodynamic simulation of galaxy formation together with an accurate ray-tracing treatment of self-shielding from the UV background and an empirical prescription for H_2 formation, to compute the $z \approx 3$ H I column density distribution function. We find agreement between the reference OWLS model and the entire column density range probed by observations ($10^{12}\,{\rm cm}^{-2} < N_{\rm H\,I} < 10^{22}\,{\rm cm}^{-2}$). We have shown that $f(N_{\rm H\,I}, z)$ flattens above $N_{\rm H\,I} = 10^{18}\,{\rm cm}^{-2}$ due to self-shielding, and steepens around $N_{\rm H\,I} = 10^{20.3}\,{\rm cm}^{-2}$ and $N_{\rm H\,I} = 10^{21.5}\,{\rm cm}^{-2}$ due to the absorbing gas becoming fully neutral, and the transition from atomic to molecular hydrogen, respectively. In future work, we will examine the systems causing this absorption in greater detail and repeat these analyses on a large sample of OWLS models.

We thank Joseph Hennawi, Matt McQuinn, Pasquier Noterdaeme, Xavier Prochaska, and the OWLS team. These simulations were run on Stella, the LOFAR Blue-Gene/L system in Groningen, and on the ICC Cosmology Machine which is part of the DiRAC Facility jointly funded by STFC, the Large Facilities Capital Fund of BIS, and Durham University as part of the Virgo Consortium research program and would not function without the extraordinary efforts of Lydia Heck. This work was sponsored by the National Computing Facilities Foundation (NCF) for the use of supercomputer facilities, with financial support from the Netherlands Organization for Scientific Research (NWO).

REFERENCES

Abazajian, K. N., Adelman-McCarthy, J. K., Agüeros, M. A., et al. 2009, ApJS, 182, 543
Bahcall, J. N., & Peebles, P. J. E. 1969, ApJ, 156, L7
Bi, H., & Davidsen, A. F. 1997, ApJ, 479, 523
Blitz, L., & Rosolowsky, E. 2006, ApJ, 650, 933
Carswell, R. F., Webb, J. K., Baldwin, J. A., & Atwood, B. 1987, ApJ, 319, 709
Cen, R., Ostriker, J. P., Prochaska, J. X., & Wolfe, A. M. 2003, ApJ, 598, 741
Cen, R. 2010, arXiv:1010.5014
Dalla Vecchia, C., & Schaye, J. 2008, MNRAS, 387, 1431
Faucher-Giguère, C., Lidz, A., Hernquist, L., & Zaldarriaga, M. 2008, ApJ, 688, 85
Gardner, J. P., Katz, N., Hernquist, L., & Weinberg, D. H. 1997, ApJ, 484, 31
Górski, K. M., Hivon, E., Banday, A. J., et al. 2005, ApJ, 622, 759
Haardt, F., & Madau, P. 2001, in Clusters of Galaxies and the High Redshift Universe Observed in X-rays, ed. D. M. Neumann & J. T. T. Van, 64 (arXiv:astro-ph/0106018)
Haardt, F., & Madau, P. 2011, arXiv:1105.2039
Haehnelt, M. G., Steinmetz, M., & Rauch, M. 1998, ApJ, 495, 647
Hong, S., Katz, N., Davé, R., et al. 2010, arXiv:1008.4242
Katz, N., Weinberg, D. H., Hernquist, L., & Miralda-Escude, J. 1996, ApJ, 457, L57
Kim, T., Carswell, R. F., Cristiani, S., D'Odorico, S., & Giallongo, E. 2002, MNRAS, 335, 555
Kohler, K., & Gnedin, N. Y. 2007, ApJ, 655, 685
Komatsu, E., Smith, K. M., Dunkley, J., et al. 2011, ApJS, 192, 18
Krumholz, M. R., Ellison, S. L., Prochaska, J. X., & Tumlinson, J. 2009, ApJ, 701, L12
McQuinn, M., Oh, S. P., & Faucher-Giguere, C.-A. 2011, arXiv:1101.1964
Nagamine, K., Choi, J.-H., & Yajima, H. 2010, ApJ, 725, L219

Nagamine, K., Springel, V., & Hernquist, L. 2004, MNRAS, 348, 421
Noterdaeme, P., Petitjean, P., Ledoux, C., & Srianand, R. 2009, A&A, 505, 1087
O'Meara, J. M., Prochaska, J. X., Burles, S., et al. 2007, ApJ, 656, 666
Péroux, C., Dessauges-Zavadsky, M., D'Odorico, S., Sun Kim, T., & McMahon, R. G. 2005, MNRAS, 363, 479
Petitjean, P., Webb, J. K., Rauch, M., Carswell, R. F., & Lanzetta, K. 1993, MNRAS, 262, 499
Pontzen, A., Governato, F., Pettini, M., et al. 2008, MNRAS, 390, 1349
Prochaska, J. X., O'Meara, J. M., & Worseck, G. 2010, ApJ, 718, 392
Prochaska, J. X., & Wolfe, A. M. 2009, ApJ, 696, 1543
Rauch, M. 1998, ARA&A, 36, 267
Razoumov, A. O., Norman, M. L., Prochaska, J. X., & Wolfe, A. M. 2006, ApJ, 645, 55
Schaye, J. 2001a, ApJ, 559, 507
Schaye, J. 2001b, ApJ, 562, L95
Schaye, J. 2006, ApJ, 643, 59
Schaye, J., & Dalla Vecchia, C. 2008, MNRAS, 383, 1210
Schaye, J., Dalla Vecchia, C., Booth, C. M., et al. 2010, MNRAS, 402, 1536
Springel, V. 2005, MNRAS, 364, 1105
Tescari, E., Viel, M., Tornatore, L., & Borgani, S. 2009, MNRAS, 397, 411
Theuns, T., Leonard, A., & Efstathiou, G. 1998a, MNRAS, 297, L49
Theuns, T., Leonard, A., Efstathiou, G., Pearce, F. R., & Thomas, P. A. 1998b, MNRAS, 301, 478
Tytler, D. 1987, ApJ, 321, 49
Wiersma, R. P. C., Schaye, J., Theuns, T., Dalla Vecchia, C., & Tornatore, L. 2009a, MNRAS, 399, 574
Wiersma, R. P. C., Schaye, J., & Smith, B. D. 2009b, MNRAS, 393, 99
Wolfe, A. M., Gawiser, E., & Prochaska, J. X. 2005, ARA&A, 43, 861
Zheng, Z., & Miralda-Escudé, J. 2002, ApJ, 568, L71
Zwaan, M. A., & Prochaska, J. X. 2006, ApJ, 643, 675